SCIENTIFIC NOTEBOOK 928E

Unsaturated Zone Flow Consistency

by

Stuart A. Stothoff

Southwest Research Institute
Center for Nuclear Waste Regulatory Analyses
San Antonio, Texas

July 1, 2010

Initial Entries

Scientific NoteBook: #928E

Issued to: S. A. Stothoff

Issue Date: April 10, 2008

Computerized Initials: SAS

This computerized Scientific NoteBook is intended to address the criteria of CNWRA QAP–001.

This scientific notebook was started to document independent investigations related to consistency of representations of flow in the unsaturated zone across different groups. The notebook was created to prepare for the Department of Energy (DOE) license application for Yucca Mountain. After receipt of the license application, such investigations became part of the Safety Evaluation Report preparation and were continued in Scientific Notebook 1005E.

The analyses in this scientific notebook use independent numerical calculations.

RL 7/7/2010

Contents

Initial Entries ii

List of Figures iv

List of Tables v

1 Flow from infiltration to the water table 1-1

04/10/08 Introduction 1-1

04/10/08 Infiltration and deep percolation 1-1

04/14/08 Thermal properties 1-3

04/17/08 Chloride and chlorine-36 1-7

04/18/08 Independent chloride mass balance model 1-11

Final QA Information i

RL 7/7/2010

List of Figures

1-1 Specific heat measured for Topopah Spring welded core samples. 1-4

1-2 Thermal conductivity for oven-dried samples. 1-6

1-3 Thermal conductivity for variably saturated below-boiling samples. 1-8

1-4 Difference in thermal conductivity between saturated and oven-dry conditions for below-boiling samples. 1-9

RL 7/7/2010

List of Tables

RL 7/7/2010

1 Flow from infiltration to the water table

04/10/08 Introduction.

SAS

Work addressing aspects of flow in the unsaturated zone has typically been partitioned into different groups, each with a different focus. As part of preparation for the license application, I am examining the consistency of data, interpretations, and models across the unsaturated zone. This is a joint project touching upon the UZ1 and UZ2 ISIs, and (time permitting) may touch upon the ENG3 and ENG4 ISIs. I am maintaining this project notebook to collect my investigations on this topic. The initial focus relates to consistency of mountain-scale flow patterns with respect to infiltration estimates. Subsequent work may examine consistency of near- and within-drift estimates with respect to infiltration and mountain-scale flow.

04/10/08 Infiltration and deep percolation.

SAS

The Sandia National Laboratories (SNL) infiltration model (Sandia National Laboratories, 2007a) is used to provide upper boundary conditions to mountain-scale simulations. The infiltration model may be considered uncalibrated, in the sense that the infiltration estimates are not compared to observations within the bedrock to develop the estimates. DOE has used a procedure to adjust the likelihood of the infiltration estimates based on comparisons of temperature and chloride observations at depth with estimates from three-dimensional (3D) mountain-scale models at the same locations (Sandia National Laboratories, 2007b).

The temperature comparison uses observations from boreholes SD-12, NRG-6, NRG-7a, UZ#5, and UZ-7a, which were obtained under a qualified QA program. Borehole UZ#4 also has observations obtained under the same program; this borehole was not used in the comparison. These observations were taken using permanently installed thermocouple pairs with periodically obtained measurements.

Bodvarsson et al. (2003) report a related analysis using a one-dimensional (1D) analytic solution for these boreholes plus an additional set of boreholes with observations reported by Sass et al. (1988). The Sass et al. (1988) measurements were obtained by moving a thermocouple within (i) the open borehole, or (ii) a water-filled pipe within the borehole. These measurements were obtained relatively soon after borehole emplacement; some were repeated several times, others were not, and I am unaware of later temperature measurements in the 35 Sass et al. (1988) boreholes. The additional boreholes include the G and H series of boreholes, the WT series of boreholes

(excluding WT-24, which was not yet drilled), boreholes a4 through a7, b1, p1, UZ-1, VH-1 and VH-2, and J-13.

Bodvarsson et al. (2003) use estimated *in situ*thermal conductivity values than appear to differ from the property set used by the thermal model. Bodvarsson et al. (2003) state that the values for borehole SD-12 were taken from the Reference Information Database; presumably the same source was used for the other boreholes as well. The values represent entire hydrostratigraphic units (*e.g.*, the TCw, PTn, etc.).

The thermal model uses thermal conductivities estimated by Bechtel SAIC Company, LLC (2004c) (for the potential repository horizons) and Bechtel SAIC Company, LLC (2004b) (for the other lithostratigraphic units). Thermal conductivity estimates for the potential repository are based on 27 core samples obtained from boreholes NRG-4, NRG-5, NRG-6, and NRG-7a, which are all in the vicinity of the north ramp of the Exploratory Studies Facility (ESF), and 6 samples obtained from Alcove 5, in the northern portion of the main drift of the ESF. These samples are all obtained from within a rectangle of approximately 0.8 by 1.8 km extent. Thermal conductivity estimates for the non-repository lithostratigraphic layers are based on 47 samples from the NRG boreholes (all of the NRG samples from the repository horizon except NRG6-354.9C/354.9B are reused) plus a total of 5 samples collected from SD-7, SD-9, and SD-12. All of the NRG and Alcove 5 samples were from the repository horizon or higher; the SD samples are all taken from the upper portion of the Calico Hills formation (Tac and Tacbt zones). All of the samples were used to determine two endpoint thermal conductivity values, representing wet (saturated) and dry conditions. The thermal model uses calculated values for saturation to linearly interpolate between these extremes.

For the purposes of a comparison analysis, I adopted the same analytic solution as used by Bodvarsson et al. (2003), which is developed by Shan and Bodvarsson (2004). The 1D solution considers conduction in several layers plus advection by moving liquid water. The analytic solution has the form

$$T_i(z) = C_{i,1} \exp(vz/\alpha_i) + C_{i,2} \tag{1-1}$$

$$\alpha_i = \frac{\lambda_i}{\rho_w c_w} \tag{1-2}$$

where i denotes the layer, T is temperature [K], v is percolation flux [L/T], z is the (downward) vertical coordinate [L], λ is thermal conductivity [J/TLK], ρ_w is liquid water density [M/L^3], and c_w is water specific heat capacity [J/MK]. Shan and Bodvarsson (2004) specify a value of 4.18×10^6 J/m^3/K for $\rho_w c_w$, which I used for my analyses. The C coefficients are integral constants for each layer, determined by imposing continuity of temperature and heat flux at the layer interfaces

plus imposed temperature or heat flux boundary conditions. For fixed top (T_0) and bottom (T_B) temperatures,

$$C_{1,1} = \frac{T_B - T_0}{a - 1} \tag{1-3}$$

$$C_{i+1}, 1 = \exp\left[vd_i\left(\frac{1}{\alpha_i} - \frac{1}{\alpha_{i+1}}\right)\right] C_{i,1} \tag{1-4}$$

$$C_{1,2} = C_{2,2} = \cdots = C_{n,2} = \frac{aT_0 - T_B}{a - 1} \tag{1-5}$$

$$a = \exp(vd_n/\alpha_e) \tag{1-6}$$

$$\alpha_e = \frac{d_n}{\sum_{i=1}^{N}(b_i/\alpha_i)} \tag{1-7}$$

where d_n is the total thickness of the N layers.

I used a combination of information to estimate layer thicknesses and thermal properties for each borehole. Lithostratigraphic information comes from the input files for the GFM2000 geologic framework model (Bechtel SAIC Company, LLC, 2004a), which contains observed contact depths for each layer in each borehole in a file called contacts00md.dat. The Attachment VII table in TDR-NBS-GS-000007 Rev 01 recommends contacts updated from the GFM3.0 model; there are several discrepancies between the table and the contacts file, which I resolved in favor of the attachment table. Contact information cannot be observed below the borehole completion depth; where borehole information is incomplete, I interpolated contact estimates from the gridded GFM2000 contacts using the borehole coordinates in the GFM2000 contact file and a special-purpose *Matlab* routine. Several of the boreholes had missing values for alluvium depth; I simply used the depth that could be inferred from the contacts in these cases.

04/14/08 Thermal properties.

SAS

The Brodsky et al. (1997) report provides most of the thermal conductivity values used in the Bechtel SAIC Company, LLC (2004c) and Bechtel SAIC Company, LLC (2004b) Analysis and Model Report (AMR)s. This report also reports measured specific heat for 10 air-dried samples, 3 for the TSw1 zone (from NRG-4) and 7 for the TSw2 zone (from NRG-5). Specific heat is not used in the 1D analytic solution, but I became familiar with the measured data anyway. In general, specific heat rises more-or-less linearly with temperature to approximately 160°C, then more-or-less becomes independent of temperature (Figure 1-1). Brodsky et al. (1997) describe the temperature dependence for specific heat of individual samples as a weighted sum of temperature raised to a power, with a value of 4 for the highest-order exponent in some cases. The higher-order terms are attributed to phase changes in some of the minerals (*e.g.*, tridymite, at 163°C).

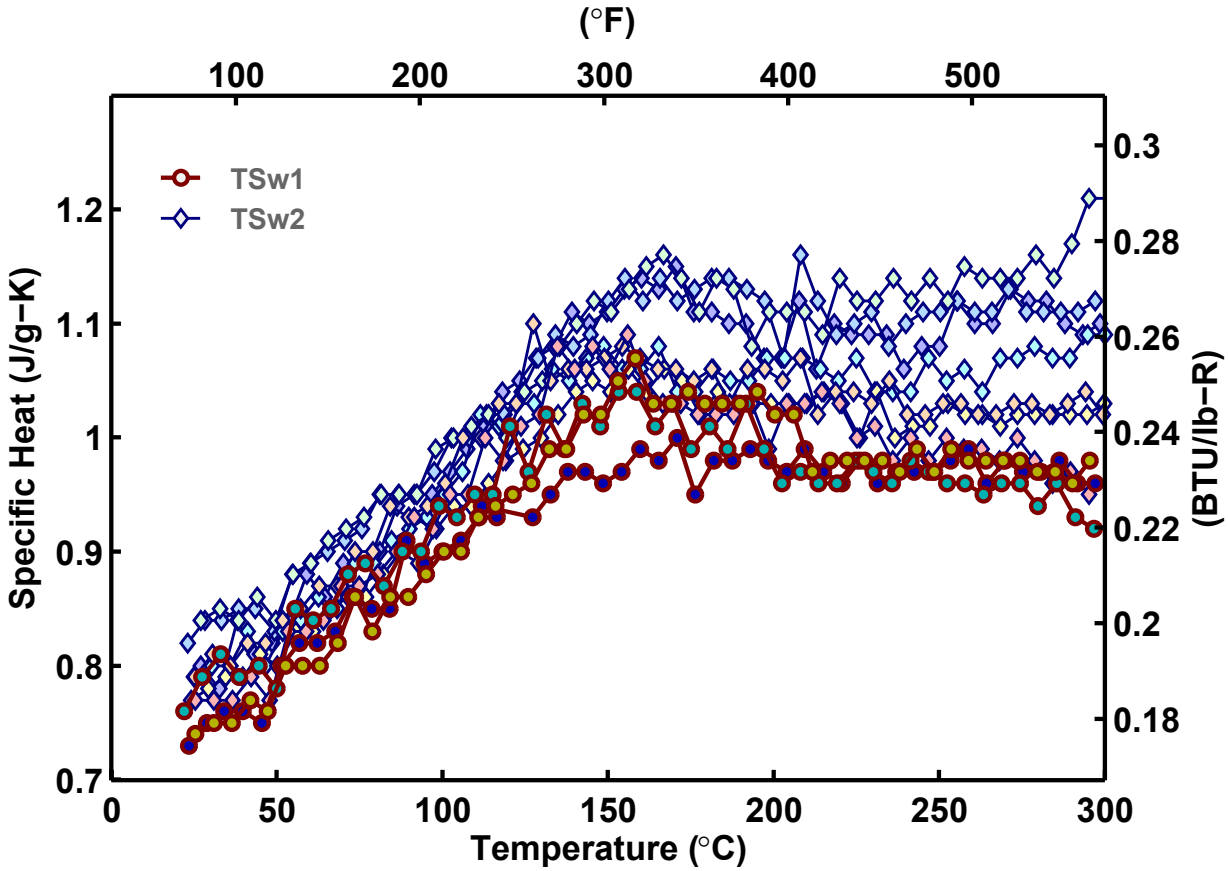

Figure 1-1: Specific heat measured for Topopah Spring welded core samples.

Unlike specific heat, a thermal conductivity value is always necessary for each stratigraphic layer when using a thermal model. The thermal conductivity approach used by the Sandia National Laboratories (2007b) thermal model uses linear interpolation of thermal conductivity between dry and wet extremes, thus requires an estimate of liquid saturation and a constitutive model for the dependence of thermal conductivity on liquid saturation. The Bodvarsson et al. (2003) analytic model does not consider liquid saturation.

I went back to the original report (Brodsky et al., 1997) providing most of the thermal conductivity values used in the Bechtel SAIC Company, LLC (2004c) and Bechtel SAIC Company, LLC (2004b) AMRs. A total of 95 core samples underwent thermal testing, with a total of 143 thermal conductivity tests (each test consisting of 3 to 7 measurements). Most samples were tested for some combination of oven-dried, vacuum-saturated, partially saturated, or air dry conditions. Oven drying occurred at 110°C held for at least 128 hr. Air-dried samples were measured in an "as-received" condition with no attempt to modify (or preserve) saturation from the original sampling.

Partially saturated samples were allowed to dehydrate at room conditions from the saturated state. Testing went in the order of air dried, vacuum saturated, partially saturated, and oven dried when multiple saturation states were considered for a given core.

Note that not all of the thermal conductivity measurements are used in the Bechtel SAIC Company, LLC (2004c) and Bechtel SAIC Company, LLC (2004b) AMRs. These AMRs only use the vacuum-saturated value(s) at 70°C and the oven-dried value(s) at 110°C to develop the estimates (these are not necessarily from the same core at a given horizon). The AMRs develop a saturation-dependent expression for bulk thermal conductivity that includes porosity. Porosity was not measured by Brodsky et al. (1997), nor was it determined for the cores, thus only the subset of thermal conductivity values is used for which an independent porosity measurement is available at the same or similar horizon.

I retyped the values from the Brodsky et al. (1997) report into an Excel spreadsheet to examine the data. Figure 1-2 displays all thermal conductivity measurements for the oven-dried samples. The TCw thermomechanical unit contains samples from the Tpcpll, Tpcplnc, and Tpcpln zones. The PTn unit contains samples from the Tpp, Tpy, Tptrv2, Tpcpv1, Tpbt2, Tpcpv, and Tpbt4 zones. The TSw1 unit contains samples from the Tptrn, Tptul, and Tptpul1 zones. The TSw2 unit contains samples from the Tptpmn3, Tptpmn2, Tptpmn1, and Tptpll zones.

Below 100°C, the measurements of thermal conductivity used a Holometrix TCA-200-LT guarded heat flow meter with data acquired and analyzed with Holometrix TCA-200-LT software. Above 100°C, the measurements of thermal conductivity used a Holometrix TCA-300 guarded heat flow meter with data acquired and analyzed with Holometrix TCA-YMP software. The samples were analyzed in order from coolest to warmest state, and some were similarly analyzed further during cooldown. Samples analyzed during both warming and cooling may have a loop indicating dual readings, but the loop is not visible for some samples that have identical readings in both directions. Samples that were analyzed by both meters are indicated with one or two gray lines between the high and low temperature regions, depending on whether the sample had a cooling cycle in the high-temperature measurement sequence.

The thermal conductivity values are similar at different temperatures. There is a trend towards slightly increasing thermal conductivity with warmer temperature for the low-temperature samples, although a few samples show declining conductivities. The cooldown thermal conductivities are consistently somewhat smaller than the warmup thermal conductivities in the high-temperature regime. Some of the samples had different measured thermal conductivities using the two flow meters, especially for the TSw2 samples.

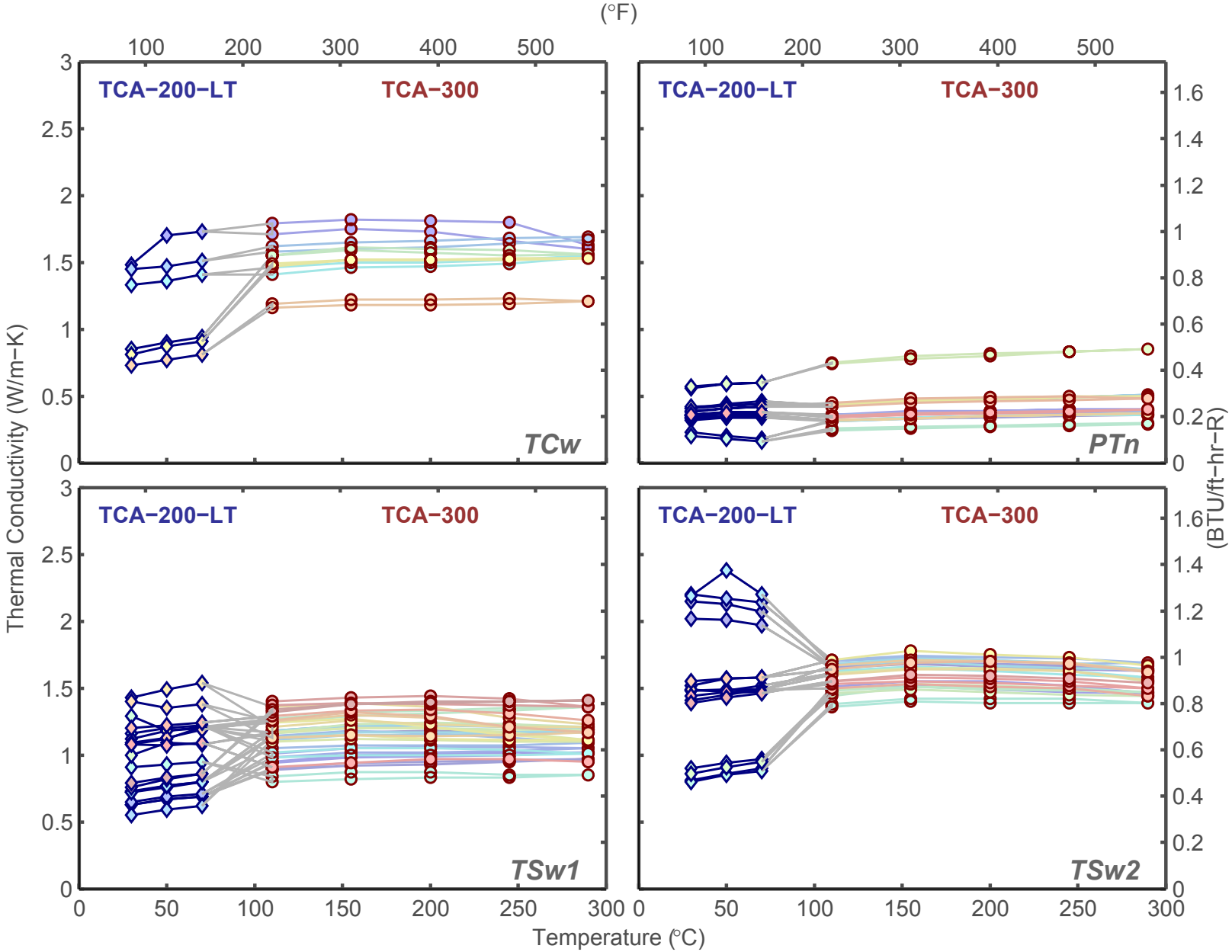

Figure 1-2: Thermal conductivity for oven-dried samples.

All of the thermal conductivity measurements below 100°C are shown in Figure 1-3, demonstrating the effect that different levels of saturation have on thermal conductivity. The vacuum-saturated samples tend to be the most conductive and the oven-dried samples tend to be the least conductive, with the partially saturated and air-dried samples falling between.

The difference between vacuum-saturated and oven-dried samples is shown in Figure 1-4. The PTn unit has a rather narrow band across all saturations, but the welded units have significantly more scatter. In the TSw2 unit, the mean difference in thermal conductivity for strata having both measurements performed on the same sample is approximately 3 times larger than for strata where different samples are used for the two measurements. The same-sample population has a mean that is more than three standard deviations larger than the mean of the different-sample population (using the different-sample population standard deviation). Interestingly, the same-sample measurements are bimodal. The TSw1 unit does not have same-sample outliers like the TSw2 unit, but the mean of the same-sample values is larger than the mean of the different-sample population by approximately 0.8 times the standard deviation of the different-sample population.

04/17/08 Chloride and chlorine-36.

SAS

Measured chloride concentration from perched waters tend to be more dilute than chloride concentrations from pore waters at the same and neighboring horizons. A DOE AMR analyzing the unsaturated zone geochemistry (CRWMS M&O, 2003) notes that the perched and pore waters have distinctly different chemical compositions. Section 7.5 of the AMR concludes that major ion concentrations and uranium isotope data suggest that the perched waters were formed by water flowing through fractures in the unsaturated zone rather than through the matrix, with compositions that are consistent with greater rates of evapotranspiration at the points where the matrix waters infiltrate the subsurface relative to the points where the perched waters infiltrate the subsurface. The AMR also suggests that perched water samples may be up to 11,000 years old based on carbon-14 and chlorine-36 ages.

The chloride mass balance model described in Section 6.5 of the Unsaturated Flow Model and Submodel (Rev03) AMR (Sandia National Laboratories, 2007b) performs chloride transport calculations using the site-scale flow models, grid, and boundary conditions. The only difference is that an additional transport equation is solved for the conservative chloride species.

The site-scale flow model applies all infiltration fluxes to the fracture continuum in the top layer. The site-scale flow model was developed to capture conditions below the PTn layer. The

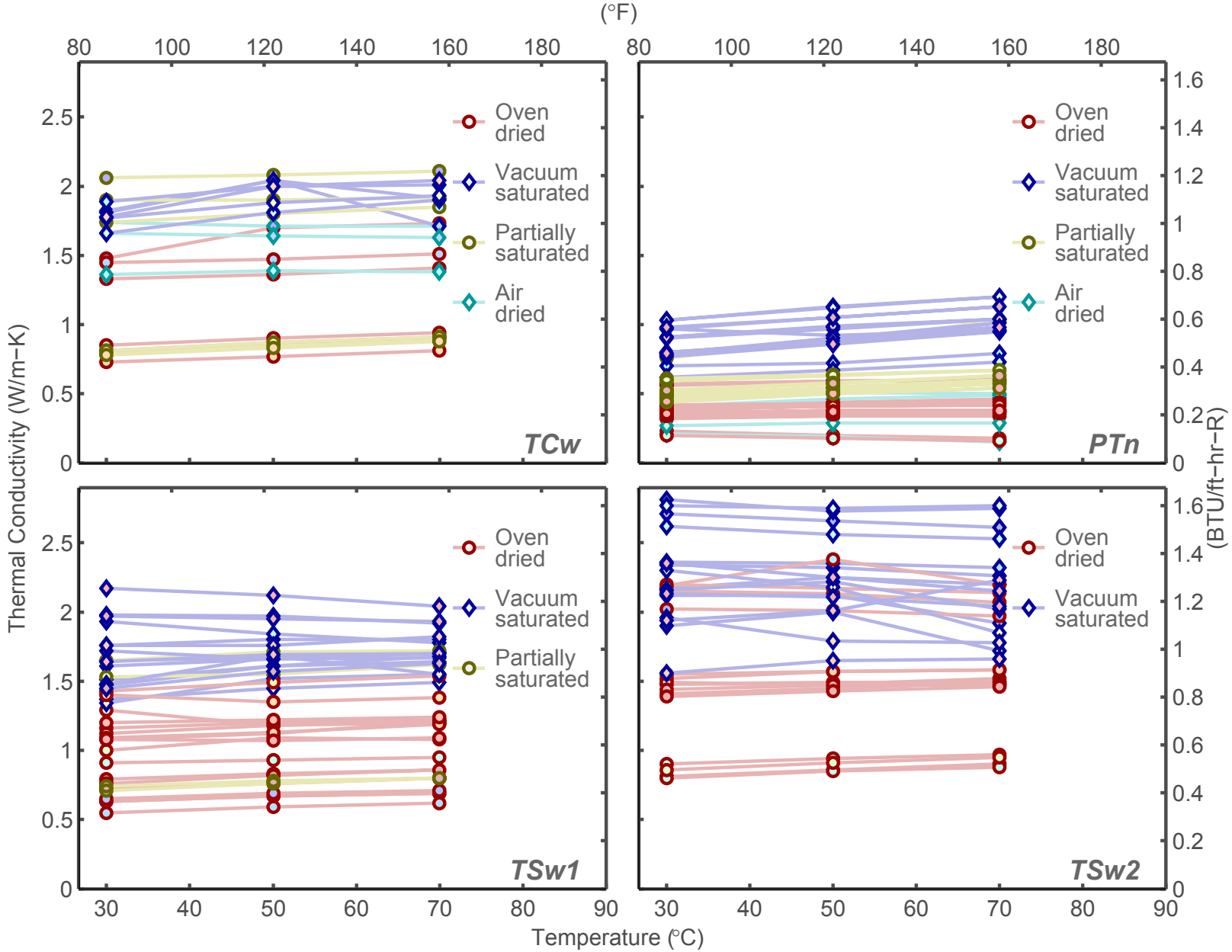

Figure 1-3: Thermal conductivity for variably saturated below-boiling samples.

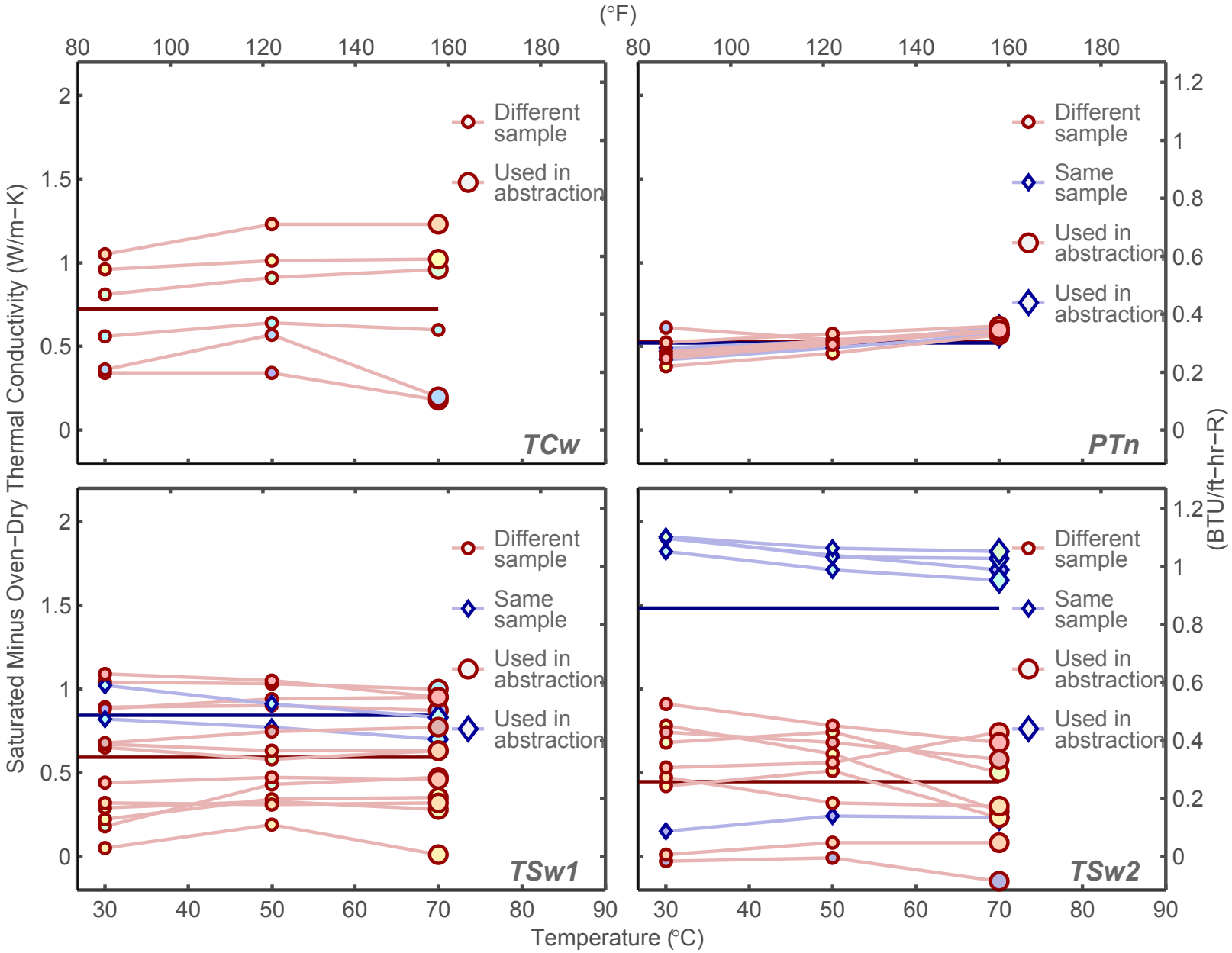

Figure 1-4: Difference in thermal conductivity between saturated and oven-dry conditions for below-boiling samples.

PTn layer is thought to draw essentially all water from the fracture system into the PTn matrix in the DOE conceptual model, and most infiltrating waters are thought to enter the bedrock in the fracture system, thus the simplification of applying all infiltration to the fracture system would presumably have little effect on calculated flow fields at and below the repository horizon.

The chloride model described by Sandia National Laboratories (2007b) uses the same assumptions for the flow field. An effective chloride concentration for precipitation is applied to the net water entering each infiltration grid cell to estimate the mass of chloride entering the top of the domain. This mass of chloride is carried into the unsaturated zone in the applied waters that enter the fracture continuum. This modeling assumption implies that water in the matrix continuum comes from the fracture continuum, thus the modeled matrix and fracture chloride concentrations should be quite similar unless there is a mechanism (such as evaporation) for differentially concentrating chloride within one of the continua.

Table 26 of the CRWMS M&O (2003) AMR tabulates average values of chloride in alluvium from boreholes UZ-N37 (133 mg/L), a large channel bottom in Wren Wash; UZ-N54 (7400 mg/L), a large channel bottom in WT-2 Wash; UZ-14 (520 mg/L), in upper Drillhole Wash; and UZ#16 (3700 mg/L), at the confluence of Antler and WT-2 Washes. The data source for these samples (DTN LA0002JF831222.001) does not appear to be included in the LSN database as of today, thus I don't know the spread in values represented by these averages. For comparison, the mean value is 59 mg/L for 56 samples from the PTn reported in the same table, with average North Ramp values of 23 mg/L (ranging from 5.7 to 69.2 mg/L), average South Ramp values of 64 mg/L (ranging from 26.5 to 103 mg/L), and average borehole values of 105 mg/L (individual values ranging from 23 through 245 mg/L).

North Ramp samples (TCw, PTn, and TSw) were obtained from stations 7+27 through 11+30. The Tcr2 or Tcr3 zones lie above stations from approximately 6+20 through 7+60 and 8+80 through 16+30. These zones are associated with high infiltration in Infiltration Tabulator for Yucca Mountain (ITYM) simulations. Samples from station 7+58 through 8+21 had concentrations of 27.9 through 69.2 mg/L. Samples from the other stations (all under the Tcr2 or Tcr3 zones) had chloride concentrations ranging from 5.7 to 20.8 mg/L.

The South Ramp PTn samples were obtained from stations 66+58 through 75+04. The lowest values (26.5 to 39.1 mg/L), at stations 66+58 through 67+21, are slightly updip of a fault at the base of a hillslope consisting of Tcpul. The higher values at 70+56 underlie a Tcpul hillslope without a mapped fault. The higher values at 74+44 through 75+04 underlie a Tcpul ridge. The Tcpul zone is relatively unfractured and is not considered to be associated with high infiltration.

Note that several samples are reported from the Main Drift of the ESF. Alcove 5, at approximately station 28+00, underlies the base of a south-facing slope in Wren Wash; most of the lower portion of the slope is mapped as Tcpll, another lithophysal zone that is not associated with high infiltration. Chloride concentrations of 111 and 133 mg/L are measured here.

Niche 3566 has values of 15.7 and 27.5 mg/L and Niche 3650 has values of 15.9 and 32.3 mg/L. Damp features not thought to be caused by construction were observed during construction of both niches (Wang et al., 1997, Section 1.3.2). The Tcpul and Tcpll zones are predominant at the ground surface above the ESF in the vicinity of the niches, although both niches are located almost directly below approximately 20-m wide bands of the Tcpmn zone. Percolating water at the niches may also be infiltrating in the nearby Sundance Fault.

Niche 3566 is located on the right rib of the ESF (west of the ESF) between the Sundance Fault intersection and a reactivated cooling joint in a reach including 5 consecutive sampled features with bomb-pulse chlorine-36, at stations 35+03, 35+08, 35+45, and 35+58 (in cooling joints), and at 35+93 (in Sundance Fault breccia). The Sundance Fault is mapped as a 274-m wide shear zone at the surface intersecting the ESF at approximately 35+90 on the right rib and 36+30 on the left rib (Kennedy et al., 1998). The discrete line survey maps a fault with 12-cm displacement at station 35+67. Approximately 100 m west of Niche 3566, the Sundance fault intersects the exposed channel bottom in the south branch of Coyote Wash.

Niche 3650 is located in more competent (less fractured) rock. Chlorine-36 measurements were not obtained in the immediate vicinity of the niche. A fault aligned with the Sundance Fault and steeply dipping to the east is mapped at the ground surface above approximately station 36+80 of the ESF (Day et al., 1998).

04/18/08 Independent chloride mass balance model. SAS

As part of the Site Environmental Impact Statement submission to Nuclear Regulatory Commission (NRC), DOE provided the flow field files used for particle tracking calculations. These 16 flow fields are the steady-state flow fields derived from the 3D site-scale model using the calibrated property sets, and presumably are identical to the flow fields used for chloride transport calculations in Section 6.5 of the Unsaturated Flow Model and Submodel (Rev03) AMR (Sandia National Laboratories, 2007b).

Using these flow fields, it is possible to test the hypothesis in the unsaturated zone geochemistry AMR (CRWMS M&O, 2003) that the matrix porewaters and perched waters have distinct

chemistries because of near-surface effects. A steady-state mixing-model analysis for chloride transport, neglecting chloride diffusion, provides an extremely efficient computational scheme when cells can be processed from upstream to downstream. The mixing model has the form

$$\sum_{i=1}^{N} q_{ii} c_i = \sum_{j=1}^{M} q_{oj} c \tag{1-8}$$

where q_{ii} is water flux entering the cell (positive in), q_{oj} is water flux exiting the cell (positive out), c_i is chloride concentration in the water entering the cell, and c is chloride concentration in the water exiting the cell. The exit concentration is

$$c = \frac{\sum_{i=1}^{N} q_{ii} c_i}{\sum_{j=1}^{M} q_{oj}} \tag{1-9}$$

When the cells are processed from upstream to downstream, all input values are known when processing the cell. The vast majority of the connections in the flow fields have both matrix and fracture flow in the direction of gravity, although a small fraction of the connections have flow opposite to gravity in one or both continua (likely due to lateral flow effects). Because flow occurs in opposite directions for some connections, it would be difficult or impossible to define a sorting order that ensures that all incoming fluxes have previously defined concentrations. Therefore, an iterative approach is taken to perform the mixing model calculations.

The simplest strategy for iteration takes advantage of the strong gravity dominance of the flow fields, simply processing cells from highest to lowest. Initial values must be imposed to account for the small subset of connections with upward flow, but the initial conditions will be obliterated upon iteration. In order to speed iteration, initial conditions are imposed that are similar to observed values. I selected 10 mg/L for the fracture continuum and 100 mg/L for the matrix continuum.

The flow fields assume that all water enters the fracture domain. In order to have separate flow paths for "fast" (fracture) and "slow" (matrix) chloride, these boundary conditions must be adjusted to provide chloride to the matrix without destroying the water mass balance. These separate flow paths may be a result of fast and dilute waters passing through the soil to reach the fractures, with slow and concentrated waters reaching the matrix. These separate flow paths may also be a result of flow concentrating processes such as evaporation from the matrix blocks near the surface, which is subject to reduced relative humidity and increased air movement relative to lower in the mountain. I am not attempting to evaluate mechanisms for initiating separate paths, just to look at the effects of separate paths on concentrations lower in the mountain.

One way to do initiate separate flow paths is to provide a miniscule water flux to the matrix with sufficiently high chloride concentration to achieve a desired chloride mass flux. With a sufficiently small water flux, the water balance would not be materially affected.

Another way to initiate flow paths in disequilibrium is to partially redistribute the initial water boundary condition (originally assigned completely to the fracture) to the matrix, adjusting the matrix-fracture transfer flux to maintain the water balance. The consistent expressions are

$$q_m = F q_b \tag{1-10}$$

$$q_f = (1 - F) q_b \tag{1-11}$$

$$q_{mf} = q_{mf0} + F q_b \tag{1-12}$$

$$q_b = q_f + q_m \tag{1-13}$$

q_f, q_m, q_{mf}, and q_b represent volumetric fluxes for the fracture continuum, matrix continuum, and total boundary conditions, respectively; q_{mf} and q_{mf0} represent the adjusted and initial matrix-fracture transfer fluxes, respectively, defined here as positive from matrix to fracture; and F represents the fraction of the total boundary flux assigned to the matrix. The calculated matrix-fracture transfer flux is from the fracture to the matrix in the vast majority of all topmost cells in the flow fields. If the water balance is achieved by making the matrix and fracture completely independent (*i.e.*, $q_{mf} = 0$), then $F = -q_{mf0}/q_b$, which can only be achieved when $q_{mf0} \leq 0$ (*i.e.*, initial matrix-fracture flow direction is from the fracture to the matrix). This criterion cannot be used in the small fraction of top cells with matrix-to-fracture transfer, because in this case F would be negative.

Regardless of the method used to initiate separate flow paths, the total chloride entering the mountain should be maintained regardless of the partitioning between fracture and matrix pathways. A simplified balance equation for a top cell is

$$q_p c_p = q_f c_f + q_m c_m \tag{1-14}$$

where q_p represents volumetric fluxes for precipitation and c_p, c_f, and c_m represent chloride concentrations in precipitation and the fracture continuum and matrix continuum boundary conditions, respectively. Measured chloride concentrations in overland flow are approximately an order of magnitude larger than the effective chloride concentration of precipitation, thus overland flow tends to flush some of the soil chloride in hillslopes into the washes. To test the effects of different flow path initiation, this flushing by overland flow is neglected.

The balance equation for the top cell is not unique without further assumptions. The value of q_p times c_p (*i.e.*, chloride deposition rate) can been estimated from observations, and the value of

q_b is imposed by the flow fields. For the purposes of the exercise, the matrix chloride concentration is assumed to be a multiple of the fracture concentration:

$$c_m = Rc_f \tag{1-15}$$

Plugging in, the chloride balance equation becomes

$$q_p c_p = (1-F)q_b c_f + Fq_b R c_f = [(1-F) + FR]q_b c_f \tag{1-16}$$

leading to

$$c_f = c_p \frac{q_p}{[(1-F) + FR]q_b} \tag{1-17}$$

$$c_m = c_p \frac{Rq_p}{[(1-F) + FR]q_b} \tag{1-18}$$

For the purposes of the exercise,

$$F = \min[1, \max(0, -q_{mf0}/q_b)] \tag{1-19}$$

implementing the assumptions that the matrix and fracture systems are generally independent if the original matrix-fracture flux is from fracture to matrix. The limits handle the rare cases for which the original matrix-fracture flux is from matrix to fracture or the original fracture-to-matrix flux exceeds the boundary flux, reflecting significant upward or lateral matrix flow. With this collection of assumptions, the R parameter is the primary adjustable parameter.

The R parameter may lead to nonphysical concentrations less than c_p if outside certain bounds. The requirement that $c_f \le c_p$ implies

$$\frac{c_f}{c_p} = \frac{1}{1 + (R-1)F}\frac{1}{f} \ge 1 \tag{1-20}$$

and the requirement that $c_m \le c_p$ implies

$$\frac{c_m}{c_p} = \frac{R}{1 + (R-1)F}\frac{1}{f} \ge 1 \tag{1-21}$$

where $f = q_b/q_p$. These constraints lead to the necessary condition

$$\frac{1-F}{1/f - F} \le R \le \frac{1-f}{fF} \tag{1-22}$$

These limits are enforced on top boundary conditions during simulations.

Matrix and fracture concentrations may also be influenced by liquid flux imbalances within a cell, which may arise from evaporation and condensation or numerical error. A number of cells

exhibit an imbalance in liquid fluxes. Local condensation, perhaps resulting from vapor flux arising from a contrast in material properties or a temperature gradient, will tend to dilute chloride in the condensing cell and concentrate chloride in the evaporating cell. Volumes with sufficiently strong condensation relative to liquid flux may end up with concentrations more dilute than is found in precipitation.

RL 7/7/2010

References

Bechtel SAIC Company, LLC. 2004a. *Geologic Framework Model (GFM2000)*. MDL-NBS-GS-000002 REV 02, Bechtel SAIC Company, LLC, Las Vegas, NV.

Bechtel SAIC Company, LLC. 2004b. *Thermal Conductivity of Non-Repository Lithostratigraphic Layers*. MDL-NBS-GS-000006 REV 01, Bechtel SAIC Company, LLC, Las Vegas, NV.

Bechtel SAIC Company, LLC. 2004c. *Thermal Conductivity of the Potential Repository Horizon*. MDL-NBS-GS-000005 REV 01, Bechtel SAIC Company, LLC, Las Vegas, NV.

Bodvarsson, G. S., E. Kwicklis, C. Shan, and Y.-S. Wu. 2003. Estimation of percolation flux from borehole temperature data at Yucca Mountain, Nevada. *Journal of Contaminant Hydrology 62–63*, 3–22.

Brodsky, N. S., M. Riggins, J. Connolly, and P. Ricci. 1997. *Thermal Expansion, Thermal Conductivity, and Heat Capacity Measurements for Boreholes UE25 NRG-4, UE25 NRG-5, USW NRG-6, and USW NRG-7/7a*. SAND95-1955, Sandia National Laboratories, Albuquerque, NM.

CRWMS M&O. 2003. *Analysis of Geochemical Data for the Unsaturated Zone*. ANL-NBS-HS-000017 Rev 00 ICN 02, Civilian Radioactive Waste Management System Management and Operation Contractor, Las Vegas, NV.

Day, W. C., C. J. Potter, D. S. Sweetkind, and C. A. S. Juan. 1998. *Bedrock geologic map of the central block area, Yucca Mountain, Nye County, Nevada*. Miscellaneous Investigations Series I-2601, United States Geological Survey, Denver, CO.

Kennedy, W. R., G. H. Neider-Westermann, and R. W. Elayer. 1998. *Geology of the Exploratory Studies Facility Topopah Spring Loop*. BAB000000-01717-0200-00002, REV01, Office of Civilian Radioactive Waste Management. MOL.19980415.0283.

Sandia National Laboratories. 2007a. *Simulation of Net Infiltration for Present-Day and Potential Future Climates*. ANL-NBS-HS-000032 REV 01, Department of Energy, Las Vegas, NV.

Sandia National Laboratories. 2007b. *UZ Flow Models and Submodels*. MDL-NBS-HS-000006 REV 03, Sandia National Laboratories, Albuquerque, NM.

Sass, J. H., A. H. Lachenbruch, W. W. Dudley, Jr., S. S. Priest, and R. J. Munroe. 1988. *Temperature, thermal conductivity, and heat flow near Yucca Mountain, Nevada: Some tectonic and hydrologic implications*. Open-File Report 87-649, United States Geological Survey, Denver, CO.

Shan, C. and G. Bodvarsson. 2004. An analytical solution for estimating percolation rate by fitting temperature profiles in the vadose zone. *Journal of Contaminant Hydrology 68*, 83–95.

Wang, J. S. Y., P. J. Cook, R. C. Trautz, R. Salve, A. L. James, S. Finsterle, T. K. Tokunaga, R. Solbau, J. Clyde, A. L. Flint, and L. E. Flint. 1997. *Field Testing and Observations of Potential Fast Flow Paths: Phase 1 Status Report of the Drift Seepage Test and Niche Moisture Study.* Level 4 Milestone SPC314M4, Lawrence Berkeley National Laboratory, Denver, CO. Accession Number MOL.19980121.0078.

RL 7/7/2010

Final QA Information

Entries into Scientific NoteBook 928E for the period April 10, 2008, to July 1, 2010, have been made by Stuart Stothoff (SAS; July 1, 2010).

No original text entered into this Scientific Notebook has been removed (SAS; July 1, 2010).

The final entry date for this Scientific Notebook is April 14, 2008, and the notebook was closed on July 1, 2010 (SAS; July 1, 2010).

RL 7/7/2010

ADDITIONAL INFORMATION FOR SCIENTIFIC NOTEBOOK NO. 928E

Document Date:	04/10/2008
Availability:	Southwest Research Institute® Center for Nuclear Waste Regulatory Analyses 6220 Culebra Road San Antonio, Texas 78228
Contact:	Southwest Research Institute® Center for Nuclear Waste Regulatory Analyses 6220 Culebra Road San Antonio, TX 78228-5166 Attn.: Director of Administration 210.522.5054
Data Sensitivity:	■"Non-Sensitive" □ Sensitive □"Non-Sensitive - Copyright" □ Sensitive - Copyright
Date Generated:	07/21/2010
Operating System: (including version number)	Windows
Application Used: (including version number)	
Media Type: (CDs, 3 ½, 5 1/4 disks, etc.)	1 CD
File Types: (.exe, .bat, .zip, etc.)	eps
Remarks: (computer runs, etc.)	Notebook supplemental material